

# Linear to Circular Polarisation Conversion using Birefringent Properties of Aligned Crystals for Multi-GeV Photons

A. Apyan,<sup>1,\*</sup> R.O. Avakian,<sup>1</sup> B. Badelek,<sup>2</sup> S. Ballestrero,<sup>3</sup> C. Biino,<sup>4,5</sup> I. Birol,<sup>6</sup> P. Cenci,<sup>7</sup> S.H. Connell,<sup>8</sup> S. Eichblatt,<sup>6</sup> T. Fonseca,<sup>6</sup> A. Freund,<sup>9</sup> B. Gorini,<sup>5</sup> R. Groess,<sup>8</sup> K. Ispirian,<sup>1</sup> T.J. Ketel,<sup>10</sup> Yu.V. Kononets,<sup>11</sup> A. Lopez,<sup>12</sup> A. Mangiarotti,<sup>3</sup> B. van Rens,<sup>10</sup> J.P.F. Sellschop,<sup>8,†</sup> M. Shieh,<sup>6</sup> P. Sona,<sup>3</sup> V. Strakhovenko,<sup>13</sup> E. Uggerhøj,<sup>14,‡</sup> U.I. Uggerhøj,<sup>15</sup> G. Unel,<sup>6</sup> M. Velasco,<sup>5,§</sup> Z.Z. Vilakazi,<sup>8,¶</sup> and O. Wessely<sup>2</sup>

(The NA59 Collaboration)

<sup>1</sup>Yerevan Physics Institute, Yerevan, Armenia

<sup>2</sup>Uppsala University, Uppsala, Sweden

<sup>3</sup>INFN and University of Firenze, Firenze, Italy

<sup>4</sup>INFN and University of Torino, Torino, Italy

<sup>5</sup>CERN, Geneva, Switzerland

<sup>6</sup>Northwestern University, Evanston, USA

<sup>7</sup>INFN, Perugia, Italy

<sup>8</sup>Schonland Research Centre - University of the Witwatersrand, Johannesburg, South Africa

<sup>9</sup>ESRF, Grenoble, France

<sup>10</sup>NIKHEF, Amsterdam, The Netherlands

<sup>11</sup>Kurchatov Institute, Moscow, Russia

<sup>12</sup>University of Santiago de Compostela, Santiago de Compostela, Spain

<sup>13</sup>Institute of Nuclear Physics, Novosibirsk, Russia

<sup>14</sup>Institute for Storage Ring Facilities, University of Aarhus, Denmark

<sup>15</sup>University of Aarhus, Aarhus, Denmark

(Dated: November 7, 2018)

We present the first experimental results on the use of a thick aligned Si crystal acting as a *quarter wave plate* to induce a degree of circular polarisation in a high energy linearly polarised photon beam. The linearly polarised photon beam is produced from coherent bremsstrahlung radiation by 178 GeV unpolarised electrons incident on an aligned Si crystal, acting as a *radiator*. The linear polarisation of the photon beam is characterised by measuring the asymmetry in  $e^+e^-$  pair production in a Ge crystal, for different crystal orientations. The Ge crystal therefore acts as an *analyser*. The birefringence phenomenon, which converts the linear polarisation to circular polarisation, is observed by letting the linearly polarised photons beam pass through a thick Si *quarter wave plate* crystal, and then measuring the asymmetry in  $e^+e^-$  pair production again for a selection of relative angles between the crystallographic planes of the *radiator*, *analyser* and *quarter wave plate*. The systematics of the difference between the measured asymmetries with and without the *quarter wave plate* are predicted by theory to reveal an evolution in the Stokes parameters from which the appearance of a circularly polarised component in the photon beam can be demonstrated. The measured magnitude of the circularly polarised component was consistent with the theoretical predictions, and therefore is in indication of the existence of the birefringence effect.

PACS numbers: 32.80, 34.80, 78.70.-g, 78.20.Fm, 42.81.Gs, 13.88.+e

Keywords: Single Crystal, Crystal Optics, Birefringence, Polarised Photons, Circular Polarization

## I. INTRODUCTION

The demand for high energy circularly polarised photon beams has increased with the need to perform experiments to determine the gluon spin density of the nucleon [1, 2, 3] from polarised photon-gluon fusion, and polarised photo production of high transverse momentum mesons [4]. A well known method to pro-

duce circularly polarised photons is from the interaction of longitudinally polarised electrons with crystalline media, where the emitted photons are circularly polarised due to conservation of angular momentum [5]. Theoretical calculations [6, 7] predict that the coherent bremsstrahlung (CB) and channelling radiation in crystals by longitudinally polarised electrons are also circularly polarised, and can be used to enhance the number of high energy circularly polarised photons. Currently, the highest energy available for polarised electrons is only 45 GeV [8, 9]. Therefore, the polarised electron beams are not sufficiently energetic to give photons that will be in the kinematic regime where  $\gamma g \rightarrow c\bar{c}$  is well above the  $\Lambda_c D$  associate production, that is, for a centre of mass energy above 70 GeV.

We have been working toward testing the conjecture

\*Now at: Northwestern University, Evanston, USA

†Deceased

‡Co-Spokeperson

§Co-Spokeperson; Now at: Northwestern University, Evanston, USA

¶Now at: University of Cape Town, Cape Town, South Africa

that it is possible to produce circularly polarised photon beams in proton accelerators using the extracted unpolarised high energy electron beams with energies of up to 250 GeV (CERN) and 125 GeV (FNAL) [10]. These unpolarised electron beams can produce linearly polarised photons via CB radiation in an aligned single crystal. One can transform the initial linear polarisation into circular polarisation by using the birefringent properties of aligned crystals. The above mentioned method was first proposed by Cabibbo and collaborators in the 1960's [11], and later the numerical calculations were done in terms of coherent pair production (CPP) [12] theory to obtain the optimal thicknesses for various cubic crystals.

One of the purposes of the NA59 collaboration was to investigate the birefringent properties of aligned crystals, and test the feasibility of producing high energy circularly polarised photon beams starting from the unpolarised 178 GeV electrons beams at CERN SPS [10]. This experiment used a consecutive arrangement of three aligned single crystals: the first crystal acted as a radiator to produce a linearly polarised photon beam, the second crystal acted as a quarter wave plate to convert the linear polarisation into circular polarisation, and the last crystal acted as an analyser to measure the change in the linear polarisation of the photon beam. The three crystal scheme used is shown in Fig. 1.

The linearly polarised photon beam was produced by CB radiation from electrons in an aligned Si <001> single crystal. The orientation of the crystal *radiator* was chosen in such a manner that the coherent peak of the photon spectrum was situated between 70-100 GeV. For the conversion of the linear polarisation into circular polarisation an aligned Si <110> crystal was used. Finally an aligned Ge <110> crystal was used as an *analyser* of the linear polarisation of photon beam.

When high energy photons propagate through a medium, the main process by which the photons are absorbed is  $e^+e^-$  pair production (PP). When photons propagate through an aligned crystal at small incident angles with respect to a crystal axis and/or a crystal plane, a coherent enhancement of the PP is manifested (CPP). The cross section for the CPP process depends on the direction of the linear polarisation of the photon beam with respect to the plane containing the crystal axis and the photon momentum (reaction plane) as shown in Fig. 1. In the experiment we used the configuration proposed in [11], where the reaction plane coincides with the crystal plane (110). Following the description given in [11], one can represent the linear polarisation of the photon beam as a superposition of two beams with polarisation directions parallel and perpendicular to the reac-

tion plane containing the photon momentum  $\mathbf{k}$  and the crystallographic axis. In this symmetric case, with respect to the plane containing the photon momentum the birefringent effect is maximum and the photon polarisation vector  $\boldsymbol{\epsilon}$  will be the combination of two unit vectors,  $\mathbf{t}$  and  $\mathbf{y}$ , parallel and perpendicular to the reaction plane, respectively:

$$\boldsymbol{\epsilon} = \epsilon_{\parallel} \mathbf{t} + \epsilon_{\perp} \mathbf{y}. \quad (1)$$

The components of the polarisation vector before and after the crystal of thickness,  $L$ , are related by a  $2 \times 2$  matrix [11, 13]:

$$\begin{pmatrix} \epsilon_{\parallel}(L) \\ \epsilon_{\perp}(L) \end{pmatrix} = \begin{pmatrix} \exp[in_{\parallel}E_{\gamma}L] & 0 \\ 0 & \exp[in_{\perp}E_{\gamma}L] \end{pmatrix} \begin{pmatrix} \epsilon_{\parallel}(0) \\ \epsilon_{\perp}(0) \end{pmatrix}$$

where  $E_{\gamma} = |\mathbf{k}|$  ( $\hbar = c = 1$ ) is the energy of the incident photon and the  $n_{\parallel}$  and  $n_{\perp}$  are complex quantities analogous to the index of refraction. As was mentioned in [11] "The diagonality is due to our choice of the basis vectors and to the symmetry of our situation in respect to the plane". The general case, when the photon momentum makes an small angle relative to the crystal plane was considered in [14, 15, 16]. The imaginary part of the index of refraction is connected with the photon absorption cross section, while the real part can be derived from the imaginary part using dispersion relations [11]. The crystal can act as a *quarter wave plate*, if the real part of the relative phases of the two components of the waves parallel and perpendicular to the reaction plane is changed by  $\pi/2$  after transmission of the photon. Thus the crystal will be able to transform the linear polarisation of the photon beam into circular polarisation at the matching thickness:

$$L = \frac{2}{\pi} \frac{1}{E_{\gamma} \Re(n_{\perp} - n_{\parallel})}. \quad (2)$$

In this paper we determine the polarisation direction with respect to the crystal radiator, and express this polarisation using Stokes parameters (with the Landau convention). Referred to our geometry the parameter  $\eta_1$  describes the linear polarisation of the beam polarised in the direction of  $45^\circ$  to the reaction plane of the radiator, while the parameter  $\eta_3$  describes the linear polarisation in the direction parallel or perpendicular to the reaction plane of the radiator. The parameter  $\eta_2$  describes the circular polarisation. The total polarisation is then written:

$$P_{\text{linear}} = \sqrt{\eta_1^2 + \eta_3^2}, \quad P_{\text{circular}} = \sqrt{\eta_2^2}, \quad P_{\text{total}} = \sqrt{P_{\text{linear}}^2 + P_{\text{circular}}^2}. \quad (3)$$

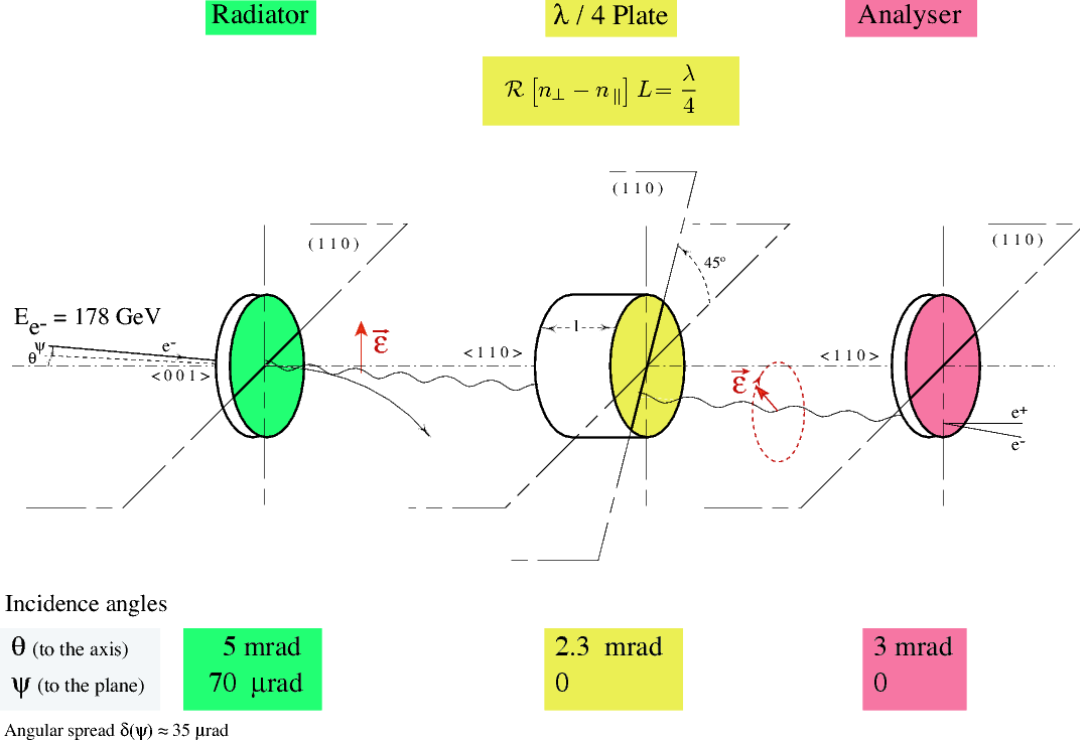


FIG. 1: Three crystal scheme.

The photon beam intensity and Stokes parameters after the quarter wave plate with the thickness  $L$  can be derived from the following formulae [17, 18]:

$$\begin{aligned}
 N(L) &= N(0)[\cosh aL + \eta_1 \sinh aL] \exp(-WL), \\
 \eta_1(L) &= \frac{\sinh aL + \eta_1(0) \cosh aL}{\cosh aL + \eta_1(0) \sinh aL}, \\
 \eta_2(L) &= -\frac{\eta_3(0) \sin bL - \eta_2(0) \cos bL}{\cosh aL + \eta_1(0) \sinh aL}, \\
 \eta_3(L) &= -\frac{\eta_3(0) \cos bL + \eta_2(0) \sin bL}{\cosh aL + \eta_1(0) \sinh aL},
 \end{aligned} \quad (4)$$

with

$$\begin{aligned}
 a &= E_\gamma \Im(n_\perp - n_\parallel) = \frac{1}{2}(W_\parallel - W_\perp), \\
 b &= E_\gamma \Re(n_\perp - n_\parallel), \quad W = \frac{1}{2}(W_\parallel + W_\perp),
 \end{aligned} \quad (5)$$

where  $W_\parallel$  and  $W_\perp$  are the pair production probabilities per unit path length for photons polarised parallel or perpendicular to the reaction plane, respectively.

As follows from equation (4), the component of the linear polarisation in the direction of  $45^\circ$  to the reaction plane of the quarter wave crystal is transformed into circular polarisation [18]. Therefore the *quarter wave plate* should be rotated by  $45^\circ$  with respect to the polar plane of the photon beam to have the optimal transformation of the polarisation. In this case the linear polarisation

component  $\eta_3$ , which was defined as the one parallel or perpendicular to the reaction plane of the radiator, represents a component of the linear polarisation in the direction of  $45^\circ$  to the reaction plane of the quarter wave plate equation (4).

As follows from equation (4), the total polarisation of the photon beam before and after the quarter wave crystal are connected by the relation:

$$P_{total}^2(L) = 1 + \frac{P_{total}^2(0) - 1}{(\cosh aL + \eta_1(0) \sinh aL)^2}. \quad (6)$$

There is conservation of polarisation if the incident photon beam is completely polarised. In a real experiment, the incident photon beam is not completely polarised, and one must seek an alternative conserved quantity. Further study of equation (4) reveals that the quantity

$$K \equiv \frac{\eta_2^2(\ell) + \eta_3^2(\ell)}{1 - \eta_1^2(\ell)} \quad (7)$$

is constant and conserved when a photon beam penetrates the quarter wave plate crystal [19] in exact symmetric orientation. This relation holds for any penetration length,  $\ell$ , between  $0 \leq \ell \leq L$  except in the case when  $\eta_2(0) = \eta_3(0) \equiv 0$  and  $\eta_1(0) = 1$ . It allows the determination of the resulting circular polarisation of photon beam by measuring its linear polarisation before and after the

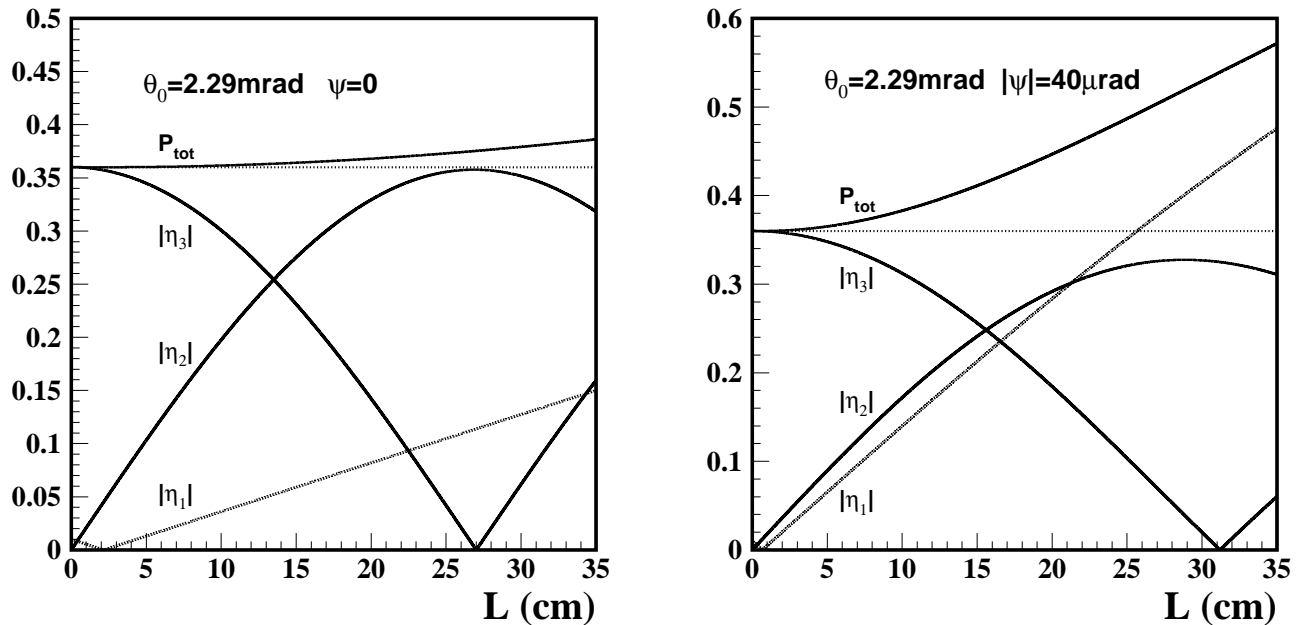


FIG. 2: Absolute values of the Stokes parameters and the total degree of polarisation for a Si crystal as a function of its thickness  $L$ , for  $E_\gamma=100$  GeV linearly polarised photons. The left hand figure and the right hand figure are calculated using initial values for the Stokes parameters described in the text. For these conditions, the crystal also acts as polariser generating a  $\eta_1$  component.

quarter wave plate. Taking into account the experimental condition, i.e. the photon beam angular divergences, one can note that  $K$  is conserved with  $\approx 5\%$  accuracy in the 80-110 GeV region as show Monte-Carlo simulations.

Fig. 2 shows the expected dependence of the Stokes parameters describing the photon polarisation as a function of the *quarter wave plate* thickness,  $\ell$ , for the surviving photons from a beam of 100 GeV. One can see 1/4 wave action. that the initial total polarisation is not conserved in the case of a partially polarised photon beam as expected from equation (6), nevertheless, the relation 6 still holds.

These calculations were carried out assuming that the Stokes parameters before the *quarter wave plate* had the following values:  $\eta_1=0.01$ ,  $\eta_2=0$  and  $\eta_3=0.36$ . In Fig. 2 (left), the photon beam makes an angle  $\theta_0=2.3$  mrad with respect to the  $\langle 110 \rangle$  axis and lies in the (110) plane ( $\psi=0$ ), while in Fig. 2 (right), the photon beam traverses the (110) plane at a small angle,  $\psi=\pm 40$   $\mu$ rad.

One can see the increase in the total polarisation,  $P_{total}$ , after the *quarter wave plate* with respect to the initial total polarisation (the straight line around 0.36). This difference comes from the fact that the aligned *quarter wave plate* can also act as a polariser. Therefore, the total polarisation behind the *quarter wave plate* can be higher than the initial polarisation. This increase is more pronounced in the case when the photon momentum makes a small angle of  $\psi=40$   $\mu$ rad with respect to the crystal plane (Fig. 2b). As described in section III C

and as shown in Fig. 2, the final calculation takes into account the beam divergence, in both the horizontal and vertical planes.

As seen from Fig. 2 the Si crystal with a thickness of  $L > 25$ cm can act as a quarter wave plate taking into account the angular divergence of the  $\gamma$ -beam. For these crystal thicknesses where the  $\eta_3(0)$  component of the initial linear photon beam polarisation will be totally transformed into the final circular component  $\eta_2(L)$ , only a few percent of the photons will survive. We defined a figure of merit (FOM), to find a compromise between the photon beam attenuation and the polarisation transformation efficiency in [10], as:

$$FOM = \eta_2(\ell)\sqrt{N(\ell)}. \quad (8)$$

Here  $N(\ell)$  is the statistical weight of the number of surviving photons. Taking into account equation (8), references [15, 16, 20] presented theoretical predictions showing the possibility of transforming the linear polarisation of a high energy photon beam into circular polarisation in the 70-100 GeV energy range. The theoretical calculations of the energy and the orientation dependence of the indices of refraction were performed using the quasi-classical operator method [16] and CPP formulae [15, 20], respectively. In these references, the optimum thickness for a *quarter wave plate* Si crystal was found to be 10 cm. The relevant geometrical parameters involved the photon beam forming an angle of 2.3 mrad from the axis (110) and the photon momentum directly in the (110) plane

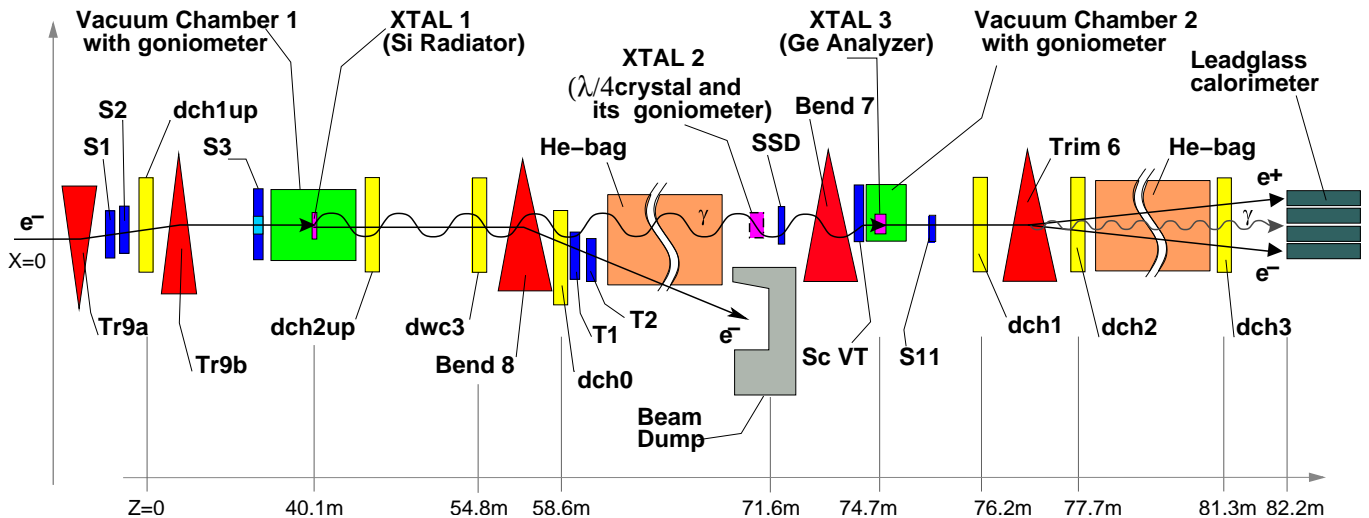


FIG. 3: NA59 experimental setup.

of Si single crystal, *i.e.* the angle between the photon momentum and crystal plane is  $\psi=0$ . For this choice of parameters, the fraction of surviving photons is 17-20%.

## II. EXPERIMENTAL APPARATUS

The NA59 experiment was performed in the North Area of the CERN SPS, where unpolarised electron beams with energies above 100 GeV are available. We took our data sample with 178 GeV electrons and an angular divergence of  $48 \mu\text{rad}$  ( $\sigma$ ) and  $35 \mu\text{rad}$  ( $\sigma$ ) in the horizontal and vertical planes, respectively.

The experimental setup used by NA59 is shown in Fig. 3.

The beam passes first through the 1.5 cm thick Si crystal *radiator*. This crystal is mounted in the goniometer located in the first vacuum chamber. The electron beam makes an angle of 5 mrad with respect to the  $\langle 001 \rangle$  axis and  $70 \mu\text{rad}$  with respect to the (100) plane. In this orientation the peak intensity of the radiated photon spectrum is around 70 GeV, and the maximum linear polarisation is  $\sim 55\%$ . Three scintillators, S1, S2 and  $\bar{S}3$  provide a coincidence signal for the primary trigger. The drift chambers Dch1up, Dch2up and the delay wire chamber Dwc3 define the incidence and exit angles of the electron beam relative to the *radiator*. The tagging system for the outgoing electron consists of the dipole magnet B8, chamber Dch0, and scintillators T1 and T2. This tagging system will only fire if the electron radiated at least 10 GeV of its initial energy due to the geometrical acceptance of scintillators T1 & T2.

The second goniometer needed to control the 10 cm thick Si  $\langle 110 \rangle$  crystal, that served as a *quarter wave crystal*, is located after the He-bag. A photograph of the *quarter wave plate* and the goniometer, at that location, is shown in Fig. 4. The orientation of this crystal relative to the photon beam was already discussed in the previ-



FIG. 4: Birefringent (*quarter wave plate*) Si crystal and goniometer.

ous section (see Table I for a summary of the crystal parameters).

The axis of the Si crystal was carefully pre-aligned with respect to the axis of the azimuthal annular stage

Crystal Type	Purpose	Axes and Planes	Orientation	Thickness
Si	Radiator	$\langle 001 \rangle$ , (110)	$\theta_0=5$ mrad, $\psi_{(110)}=70$ $\mu$ rad	1.5 cm
Si	Quarter Wave Plate	$\langle 110 \rangle$ , (110)	$\theta_0=2.3$ mrad, $\psi_{(110)}=0$	10 cm
Ge	Analyser $\eta_1$ measurement $\eta_3$ measurement	$\langle 110 \rangle$ , (110)	$\theta_0=3$ mrad, $\psi_{(110)}=0$ roll wrt radiator = $\pi/4$ , $3\pi/4$ roll wrt radiator = $0$ , $\pi/2$	1 mm

TABLE I: Where  $\theta_0$  is the angle between the photon momentum and crystal axis and  $\psi$  is the angle between the photon momentum and the indicated crystal plane.

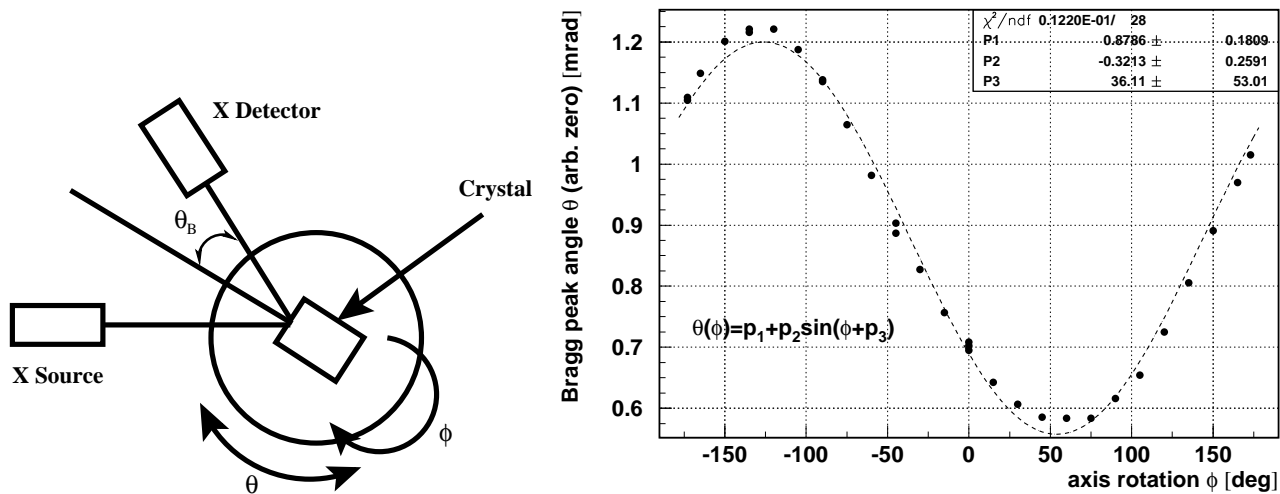


FIG. 5: Procedure and results for the annular stage alignment used to rotate the *quarter wave plate* crystal around the crystal axis.

that was subsequently mounted into the main goniometer. This pre-alignment procedure was carried out at ESRF, Grenoble. A schematic of the alignment setup and the results are shown in Fig. 5. An X-ray reflection satisfying the Bragg condition was used to monitor the orientation of the the (110) crystallographic plane which is perpendicular to the  $\langle 110 \rangle$  axis. The crystal was rolled in steps using the azimuthal goniometer stage ( $\phi$  angle rotation). The  $\langle 110 \rangle$  crystallographic axis was slightly misaligned with the crystal physical longitudinal axis and therefore also initially slightly misaligned with the the azimuthal annular stage longitudinal axis. At each azimuthal step the Bragg condition had therefore to be recovered by adjustments to the angle of crystal face using a second goniometer ( $\theta$  angle rotation). The Bragg condition was recognised by locating the two points at half-maximum of the Bragg peak. From a plot of the adjustment angle  $\theta$  for each step in the roll angle  $\phi$  of the azimuthal goniometer, the precise offset angles between the azimuthal goniometer longitudinal axis and the  $\langle 110 \rangle$  crystallographic axis could be obtained. As the thick Si crystal was mounted in the azimuthal stage by adjustment screws, the  $\langle 110 \rangle$  crystallographic axis could then be brought into coincidence with the longitudinal axis of the azimuthal goniometer.

The magnet B7 served as a sweeping magnet of the particles produced by electromagnetic showers in the *quarter wave plate*.

The scintillator Sc VT rejects radiation events coming from the conversion of the tagged photon beam upstream of the crystal *analyser*. This scintillator is mounted in front of the third goniometer used for the Ge crystal. The 1 mm thick Ge crystal served as a linear polarisation *analyser* with the photon beam momentum making an angle of 3 mrad with respect to the  $\langle 110 \rangle$  axis and it also lies within the (110) plane. The mechanisms of operation of the *analyser* was based on a measurement of the PP asymmetry, for conditions where the *analyser* crystal had the orientation just mentioned and/or perpendicular to it. The goniometer allows the crystal rotation around three axes – vertical, horizontal and around the beam direction – where one step is corresponds to a rotation of  $5 \mu$ rad. The S11 scintillator was used to detect the photon conversion into  $e^+e^-$  pairs at the *analyser* and it measured the number of charged particles seen right after the crystal *analyser*. For the analysis, we only used events with 2MIPs in S11, as a signature for PP events. The pair spectrometer consists of three drift chambers Dch1, Dch2, Dch3 and the dipole magnet Tr6. The trajectories of the  $e^+e^-$  pairs created in the *analyser* are

tracked by the drift chambers, and the momentum reconstruction of the pair gives us the momentum of the incident photon. The total radiated energy is measured by the lead glass array consisting of 13 lead glass detectors (LG).

The various plastic scintillators, that we have already mentioned above, were used to calibrate the tracking chambers and to define different physics triggers. The *norm*-trigger consisted of S1·S2·S3 to ensure that an electron is headed in the allowed direction of the *radiator* crystal. The *rad*-trigger was defined as *norm*·(T1.or.T2)·VT to show that the incoming electron has radiated and had been successfully bent out of the photon beam line. The *pair*-trigger was constructed as *rad*·S11 to select the events for which at least one  $e^+e^-$  pair was created inside the analyser crystal.

A solid state detector SSD ( $500\ \mu\text{m}$  thick Si crystal,  $5\times 5\ \text{cm}^2$ ) was placed right after the *quarter wave crystal* during dedicated runs in order to study the shower development.

Further details about the setup and the crystal alignment are given in [21].

### III. RESULTS AND DISCUSSION

The experiment was performed in two stages. In the first stage we studied in detail the linear polarisation of the photon beam, see Ref. [21]. In the second stage, the *quarter wave plate* crystal was introduced between the *radiator* and *analyser* crystal to investigate the transformation of the linear polarisation of the photon beam into circular polarisation. In this section, we describe first the method used to measure the linear polarisation, followed by a summary of the results presented in Ref. [21], and then present the *quarter wave plate* results. The linear polarisation measurements are important and mentioned here because the technique of identifying circular polarisation is related to a reduction in linear polarisation and the conservation of polarisation.

#### A. Polarisation measurement method

Both the  $\eta_1$  and  $\eta_3$  Stokes parameters described the linear polarisation of the photon beam, and were measured using a Ge crystal as an *analyser* with the method proposed in Ref. [22]. For the polarisation measurement, the experimentally relevant quantity is the asymmetry,  $A$ , between the PP cross sections,  $\sigma$ , of parallel and perpendicularly polarised photons, where the polarisation direction is measured with respect to a particular crystallographic plane of the *analyser* crystal. This asymmetry is related to the linear polarisation of the photon,  $P_1$ , through:

$$A \equiv \frac{\sigma(\gamma_{\perp} \rightarrow e^+e^-) - \sigma(\gamma_{\parallel} \rightarrow e^+e^-)}{\sigma(\gamma_{\perp} \rightarrow e^+e^-) + \sigma(\gamma_{\parallel} \rightarrow e^+e^-)} = R \times P_1, \quad (9)$$

where  $R$  is the so called ‘‘analysing power’’ of the *analyser* crystal. The quantity  $R$  corresponds to the asymmetry of a 100% linearly polarised photon beam, and it can be computed reliably [21].

If we assume that the efficiencies and acceptances are the same between the *pair*-trigger and the beam intensity normalisation trigger, taken from the *rad*-trigger, then the cross section measurement in equation (9) reduces to counting these events separately, and the measured asymmetry can be written as:

$$A = \frac{p_{\perp}/n_{\perp} - p_{\parallel}/n_{\parallel}}{p_{\perp}/n_{\perp} + p_{\parallel}/n_{\parallel}}, \quad (10)$$

where  $p_{\perp}$  and  $p_{\parallel}$  are the number of pairs produced in the perpendicular and parallel data configurations, while  $n_{\perp}$  and  $n_{\parallel}$  are the corresponding normalisation events.

#### B. Linearly Polarised Photon Beam – Aligned Radiator

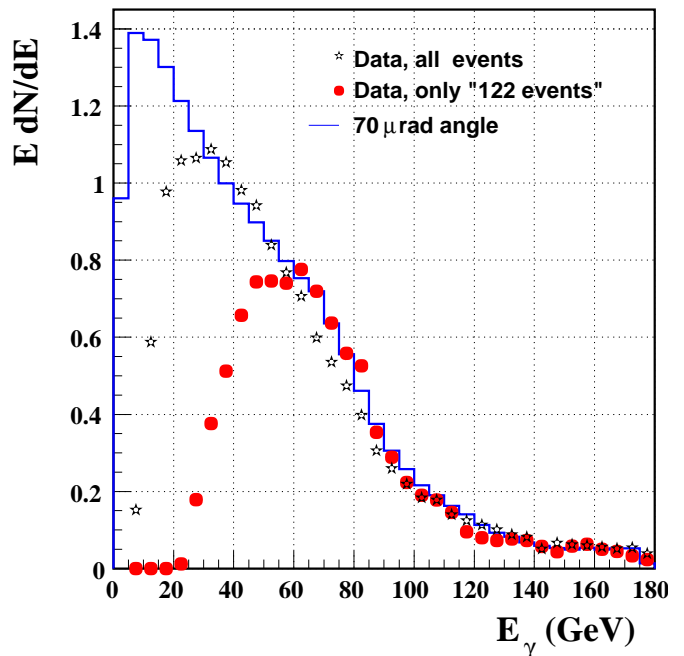


FIG. 6: Single photon intensity without a *quarter wave plate*. The label ‘‘122 events’’ refers to the cleanest ones with one hit in the chamber before the spectrometer magnet ( $e^+e^-$  pair are together), and two in both the second and third downstream drift chambers ( $e^+e^-$  pair are bend in opposite direction by the spectrometer magnet, and therefore give two distinct signals in the bending plane).

The expected and measured single photon spectrum for the chosen CB parameters for the *radiators* is shown in Fig. 6. It is evident that there is a good agreement between them.

The expected polarisation for the same set of parameters is given in Fig. 7 as a function of the single photon

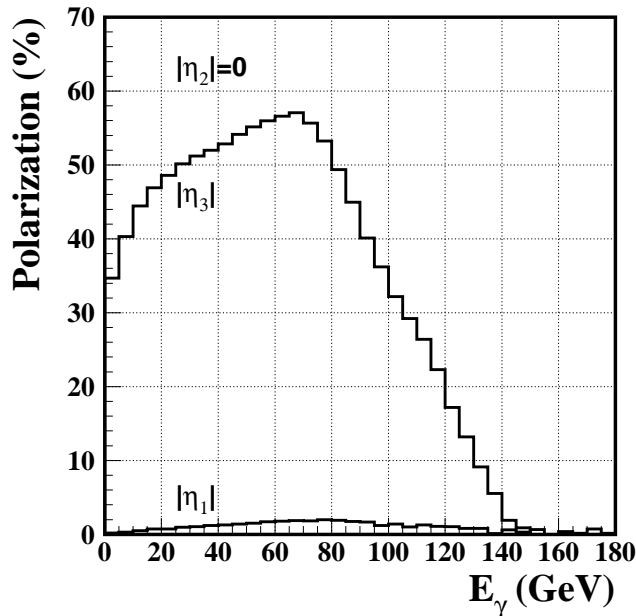


FIG. 7: Stokes parameters without a *quarter wave crystal*.

energy. As shown in reference [21], we have confirmed from our polarisation measurements the degree of polarisation for the  $\eta_1$  and  $\eta_3$  component.

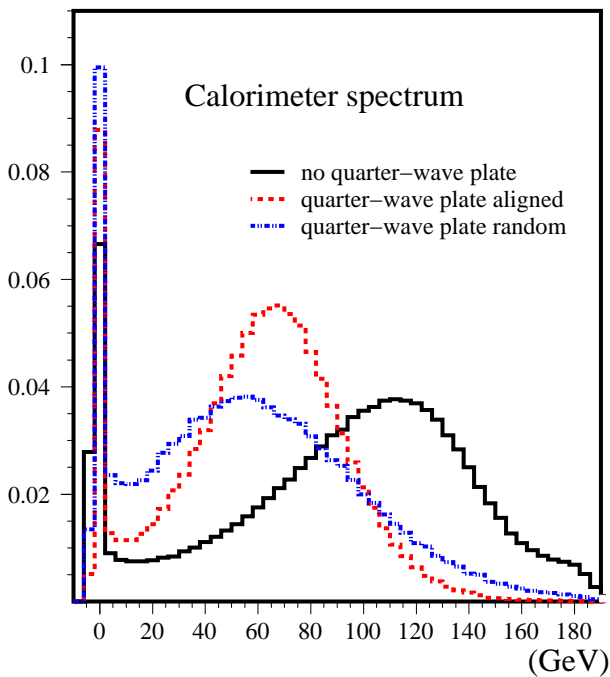


FIG. 8: Change in measured calorimeter energy spectrum for different settings of the *quarter wave crystal*. The shift in the peak energy is clear.

The most important facts from our previous measurements are: (1) there is a good agreement for the expected

single photon spectrum, therefore any change in the single photon spectrum after adding the *quarter wave crystal* reflects how the incoming photons are absorbed or transformed by it; (2)  $\eta_1$  was found to be consistent with zero, therefore any nonzero value observed after adding the *quarter wave crystal* is a reflection of birefringent effects of the crystal.

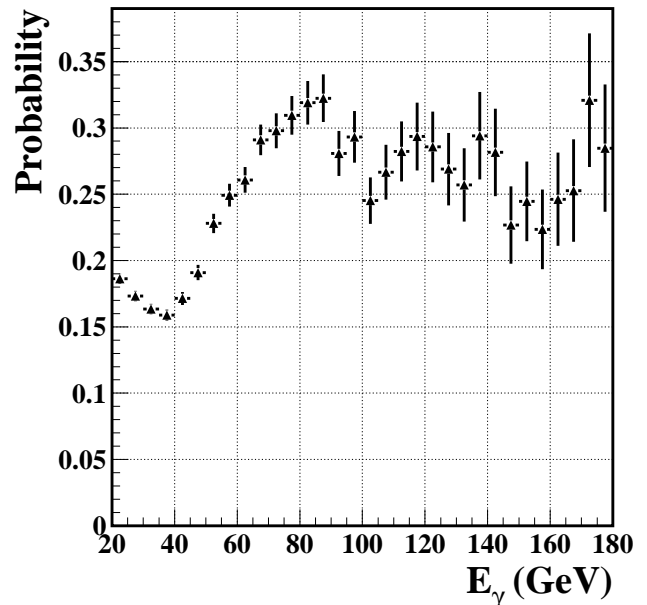


FIG. 9: Absorption probability found from the ratio of the single photon spectrum for the data with and without the *quarter wave crystal*, see Fig. 6.

### C. Elliptically polarised photon beam – Aligned Radiator & Quarter Wave Crystal

The birefringent properties of the oriented single crystal are investigated by letting the linearly polarised photon beam pass through the 10 cm thick Si crystal. Detailed theoretical calculations and simulations have been done to choose the crystal type, orientation and optimal thickness. That analysis took into account the real experimental parameters including the angular spread of the incident photon beam, the generation of secondary particles, multiple Coulomb scattering, and all particles produced by electromagnetic showers were also taken into account. In the simulation we assume the angular spread of the photons with energies between 70-100 GeV to be about  $\sim 60 \mu\text{rad}$  and  $\sim 45 \mu\text{rad}$  in horizontal and vertical planes, respectively, as measured from the data. The calculations also include the polarisation transformation part for the surviving photon beam, resulting in elliptical polarisation.

Fig. 8 shows the photon beam spectrum measured with the LG electromagnetic calorimeter. The calorimeter



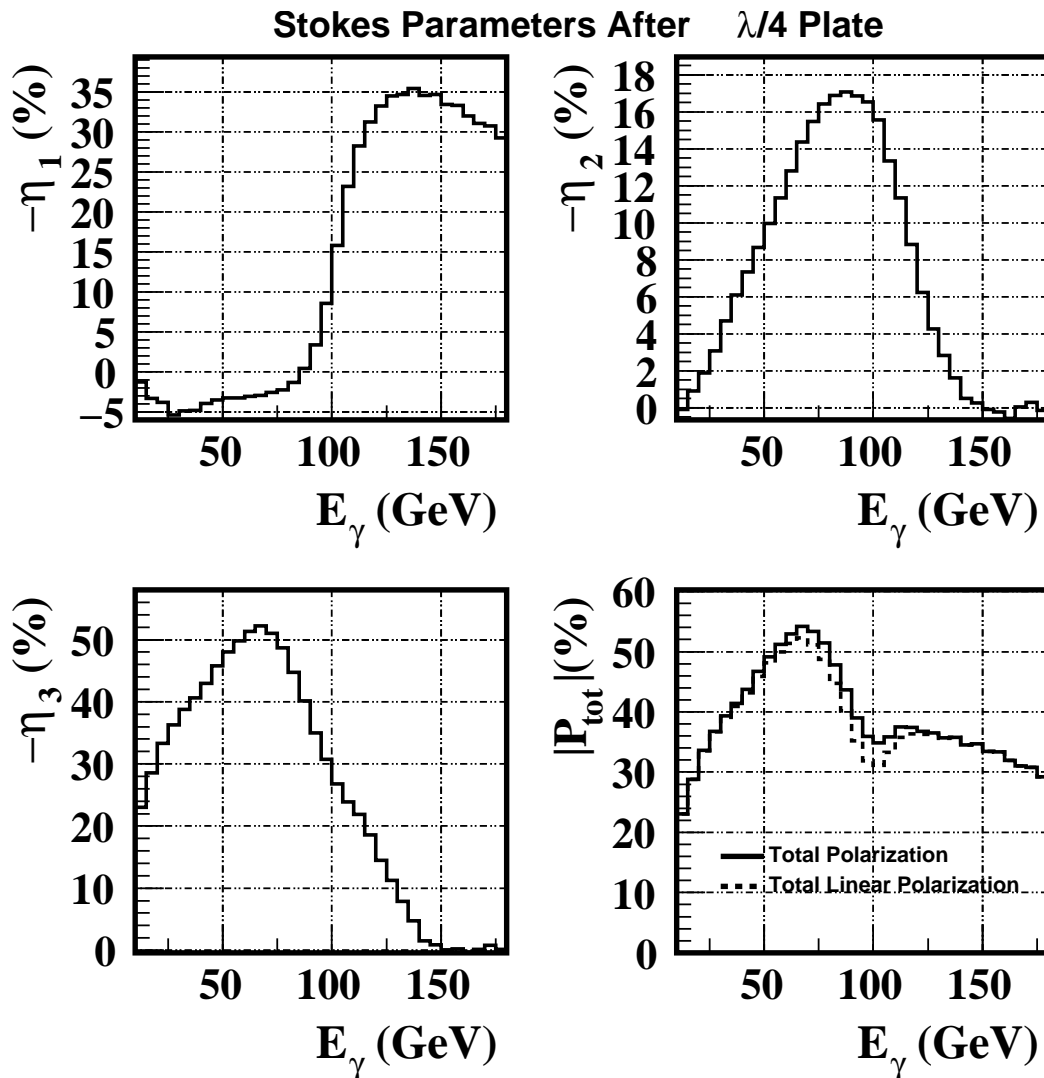


FIG. 10: Stokes parameters after the *quarter wave crystal*, assuming as input the values given in Fig. 7.

sees all the surviving photons radiated by the parent electron. By comparing the spectrum with the *quarter wave crystal* at random and/or aligned with the case in which there is no *quarter wave crystal*, we can see that the *quarter wave plate* consumes a significant amount of the beam. This causes the peak energy of the pileup spectrum to be reduced by at least 50 GeV. However, it is also clear that the energy of the photons absorbed by the *quarter wave crystal* depends on its alignment condition.

As already mentioned, the prediction is that only 17-20% of the photons will survive in our energy region. This is confirmed by the data, see Fig. 9. In addition, it is clear that the survival probability is also energy dependent as expected.

Another consequence of adding the *quarter wave crystal* is a significant increase in the photon multiplicity of an event. For example, we expect an average multiplicity of three photons per electron for the nominal *radi-*

*ator* settings. By analysing the correlation between the calorimeter spectrum and the single photon spectrum, we can conclude that the majority of these photons have energies  $<5$  GeV, and that the calorimeter events at high energies are dominated by a single high energy photon and not due to the pileup of many low energy photons. As a consequence, the measurement of the Stokes parameters in the high energy range can be performed by measuring the asymmetry using either the calorimeter or the pair spectrometer.

The expected Stokes parameters and the total polarization of the photons after the *quarter wave crystal* are given in Fig. 10. As shown, the expected value of the  $\eta_3$  Stokes parameter decreases from 36% to 30% around 100 GeV. This difference should be seen in the PP asymmetry. The expected degree of circular polarisation is of the order of  $\sim 16\%$  at the same energy. In Fig. 10, we expect an interesting increase of up to a factor of seven for the  $\eta_1$  Stokes parameter in the same energy region. This

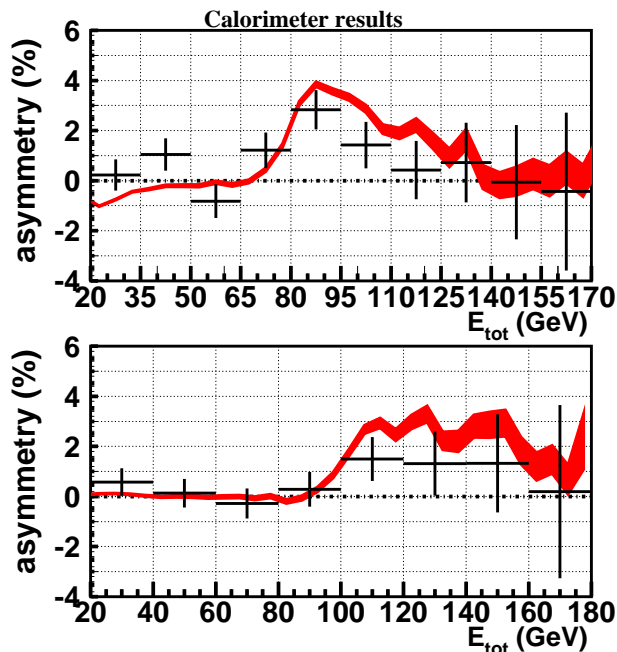


FIG. 11: Asymmetry measured with the calorimeter. The results reflects the changes in  $\eta_3$  (top) and generation of  $\eta_1$  (bottom) due to the presence of the *quarter wave crystal*.

phenomenon was also predicted by Cabibbo [23], the unpolarised photon beam traversing the aligned crystal becomes linearly polarised. This follows from the fact that the high-energy photons are mainly affected by the PP process. This cross section depends on the polarisation direction of the photons with respect to the plane passing through the crystal axis and the photon momentum (polarisation plane). Thus, the photon beam penetrating the oriented single crystal feels the anisotropy of the medium. For the experimental verification of this phenomenon with photon beams at energies of 9.5 GeV and 16 GeV, see [24, 25]. In the high energy region  $>100$  GeV the difference between the PP cross sections parallel and perpendicular to the polarisation plane is large. Since the photon beam can be regarded as a combination of two independent beams polarised parallel and perpendicular with respect to the polarisation plane, one of the components will be absorbed to a greater degree than the other one, and the remaining beam becomes partially linearly polarised.

The data taking was limited to 18 hours due to a breakdown in the SPS that lead to a six day shutdown. As a consequence, we have a small data sample to test the predictions described above. The measured asymmetries using the calorimeter are given in Fig. 11 and again using the pair-spectrometer in Fig. 12. In order to reduce systematic uncertainties, the angular settings of the *radiator* crystal (hence the direction of linear polarisation of photon beam) were kept constant, and only the *analyser* crystal was rolled around its symmetry axis to obtain the parallel and perpendicular configurations. Therefore, to

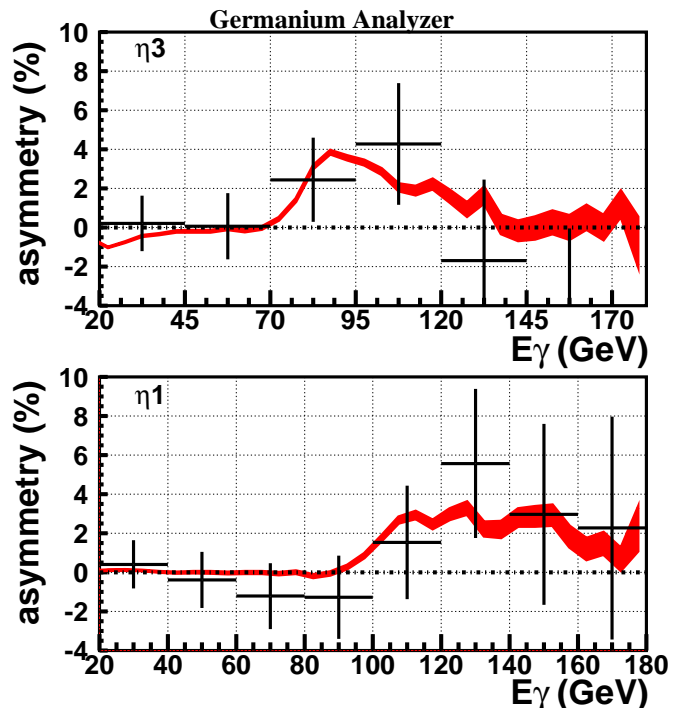


FIG. 12: Asymmetry measured with the pair spectrometer. The data sample with a fully reconstructed single  $e^+e^-$  pair is ten times smaller than the total data sample with at least one pair passing all the data quality cuts and with a 2MIPs cut in S11.

measure the polarisation of the  $\eta_3$  ( $\eta_1$ ) component, the asymmetry between the  $0$  ( $\pi/4$ ) and  $\pi/2$  ( $3\pi/4$ ) *analyser* orientations were used.

As shown in these figures, the measured asymmetries are in agreement with the predicted polarisation for the chosen Ge *analyser* crystal setting [21]. For the Stokes parameter  $\eta_3$ , the measured asymmetry after the *quarter wave crystal* is about  $2.9 \pm 0.7\%$  in the energy range between 80-100 GeV. The estimated analysing power  $R$  for the Ge *analyser* in the same energy range is about 10.4% [21]. Using the equation (9) one can estimate the measured Stokes parameter  $\eta_3$  after the *quarter wave crystal*. Thus, the measured Stokes parameter is  $\eta_3 = 28 \pm 7\%$  (see Fig. 10). For the Stokes parameter  $\eta_3$ , the measured asymmetry without the *quarter wave crystal* in the same energy range was found to be  $4.7 \pm 1.7\%$ , (see [21]). This corresponds to a measured value of  $\eta_3 = 44 \pm 11\%$ , which is also consistent with the theoretically expected value of  $\eta_3$ , see Fig. 7. The experimental measured and predicted degree of linear polarization (Stokes parameters  $\eta_1$  and  $\eta_3$ ) are presented in [26].

Similar calculations may be done for the Stokes parameter  $\eta_1$ . If we make a weighted average for the asymmetry values between 20 and 100 GeV, where we expect no asymmetry, we obtain a value of  $0.19 \pm 0.3\%$ . Above 100 GeV we expect a small asymmetry, where we measured  $(1.4 \pm 0.7)\%$  between 100 and 180 GeV.

Using the equation (7) one can now find the measured circular polarization degree which is equal  $\eta_2=21\pm 11\%$ . This is consistent with the predicted value of 16%.

The statistical significance of the result was estimated using the F-test to evaluate the confidence level associated with distinguishing between two different statistical distributions. The first distribution was formed by the variance of the energy dependent data for the experimental circular polarisation with respect to the theoretical prediction displayed in Fig. 10. The second distribution was formed by the variance of the same data to the null hypothesis prediction of no circular polarisation. Limiting the test to the region where the crystal polarimeter has analysing power, and also to the region where the circular polarimetry technique of equation 7 has efficiency (80 - 110 GeV), then we find a confidence limit of 73% for the observation of circular polarisation.

#### IV. CONCLUSION

The experimental results show that the aligned single crystals are unique tools to produce polarized high-energy photon beams and for measuring its polarization degree. Coherence effects in single crystals can be used to transform linear polarization of high-energy photons into circular polarization and vice versa. Thus, it seems possible to produce circularly polarized photon beams with energies above 100 GeV at secondary (unpolarized) electron beams at high energy proton accelerators. The birefringent effect becomes more pronounced at higher photon energy, which allows for thinner crystals with higher transmittance. Existing diamond arrays have already the appropriate quarter lambda thickness of about 2 cm and will have a transmission probability of about 80% for 100 GeV photons. Such a diamond array that could act as

a *quarter wave crystal* was produced for our collaboration and was aligned and used as a linear polarization analyser, see Ref. [21].

We did not perform a direct measurement of the circular polarization by measuring the asymmetry of  $\rho$ -meson decays, which would have needed additional beam time. However, realistic theoretical calculations describe very well the radiated photon spectrum from the aligned radiator and the pair production asymmetries in the aligned analyser both with and without the birefringent Si crystal in the photon beam. In view of this good agreement the predicted birefringent effect seems to be confirmed by the present measurements. Measurements of the charged particle multiplicity with depleted Si detectors show a large sensitivity to crystal alignments and can be used to control the alignment of crystals and photon polarization in a future polarimeter set-up.

#### Acknowledgments

We dedicate this work to the memory of Friedel Sell-schop. We express our gratitude to CNRS, Grenoble for the crystal alignment and Messers DeBeers Corporation for providing the high quality synthetic diamonds. We are grateful for the help and support of N. Doble, K. Elsener and H. Wahl. It is a pleasure to thank the technical staff of the participating laboratories and universities for their efforts in the construction and operation of the experiment.

This research was partially supported by the Illinois Consortium for Accelerator Research, agreement number 228-1001. UIU acknowledges support from the Danish Natural Science research council, STENO grant no J1-00-0568.

- 
- [1] G. Baum et al., Compass Proposal, CERN/SPSLC 96-14, SPSLC/P297 (1996).
  - [2] Proposal on Spin Physics Using the RHIC Polarized Collider (RHIC-Spin Collaboration) (1992), update 1993.
  - [3] V. Ghazikhanian et al., SLAC Proposal E-159/160/161 (2000).
  - [4] A. Afanasev, C. E. Carlson, and C. Wahlquist, Phys. Rev. D **58**, 054007 (1998).
  - [5] H. Olsen and L. C. Maximon, Phys. Rev. **114**, 887 (1959).
  - [6] I. M. Nadzhafov, Bull. Acad. Sci. USSR, Phys. Ser. **14**, 2248 (1976).
  - [7] A. B. Apyan et al., Nucl. Instrum. Methods Phys. Res. B **145**, 142 (1998).
  - [8] R. Alley et al., Nucl. Instrum. Methods Phys. Res. A **365**, 1 (1995).
  - [9] J. L. Turner et al., Presented at EPAC'02, SLAC-PUB-9235 (2002).
  - [10] A. Apyan et al., Proposal to the CERN SPS Committee, CERN/SPSC 98-17, SPSC/P308 (1998).
  - [11] N. Cabibbo et al., Phys. Rev. Lett. **9**, 270 (1962).
  - [12] M. L. Ter-Mikaelian, *High Energy Electromagnetic Processes in Condensed Media* (Wiley Interscience, New-York, 1972).
  - [13] G. D. Zorzi et al., in Polarization at LEP **2**, 64 (1988).
  - [14] V. A. Maisheev, V. L. Mikhalev, and A. Frolov, Sov. Phys. - JETP **74**, 740 (1992).
  - [15] V. A. Maisheev, hep-ex/9904029.
  - [16] V. M. Strakhovenko, Nucl. Instrum. Methods Phys. Res. B **173**, 37 (2001).
  - [17] V. N. Baier, V. M. Katkov, and V. M. Strakhovenko, Nucl. Instrum. Methods Phys. Res. B **35**, 21 (1988).
  - [18] V. N. Baier, V. M. Katkov, and V. M. Strakhovenko, *Electromagnetic Processes at High Energies in Oriented Single Crystals* (World Scientific, Singapore, 1998).
  - [19] Y. V. Kononets, (private communication).
  - [20] N. Z. Akopov, A. B. Apyan, and S. Darbinyan, hep-ex/0002041.
  - [21] A. Apyan et al., hep-ex/0306028.
  - [22] G. Barbiellini et al., Nuovo Cimento **28**, 435 (1963).
  - [23] N. Cabibbo et al., Nuovo Cimento **27**, 979 (1963).

- [24] C. Berger et al., Phys. Rev. Lett. **25**, 1366 (1970).
- [25] R. L. Eisele et al., Nucl. Instrum. Methods Phys. Res. **113**, 489 (1973).
- [26] A. Apyan et al., Nucl. Instrum. Methods Phys. Res. B (to be published).